CC BY NC ND

Increasing the efficiency of vertical-axis turbines through improved blade support structures

Thierry Villeneuve[a,1], Grégoire Winckelmans[b], Guy Dumas[a]

[a] *CFD Laboratory LMFN, Département de génie mécanique, Université Laval, Québec, QC, Canada, G1V 0A6*
[b] *Institute of Mechanics, Materials and Civil Engineering (iMMC), Université catholique de Louvain (UCLouvain), 1348 Louvain-la-Neuve, Belgium*

Postprint, 2021 - Renewable Energy
Published version available online at: https://doi.org/10.1016/j.renene.2021.01.092

Abstract

The impact of the blade support structures (the struts) on the performance of vertical-axis turbines at a high Reynolds number is investigated here. Numerical simulations of a single-blade turbine with different strut configurations are carried out and the results are compared to a reference hypothetical turbine without strut. The results show that the struts are less detrimental to the turbine efficiency if they are located at the tips of the turbine blade, rather than at other intermediate positions along the blade span. Moreover, for struts located at the blade tips, it is shown that using rounded junctions between the struts and the blade can lead to a significant increase in the turbine efficiency. Indeed, the best turbine configuration presented in this paper has an efficiency that is more than 20% larger than that of the reference turbine without strut. This important increase in the turbine efficiency can partly be attributed to the fact that the tip struts with rounded junctions act as efficient winglets, leading to a significant decrease in the induced drag on the turbine blade. The results presented show that well-designed blade support structures can be very beneficial to the performance of vertical-axis turbines.

Keywords: Cross-flow turbine, H-Darrieus turbine, VAWT, Blade mounting structures, Arms, Induced drag

1. Introduction

In the wind and hydrokinetic energy sectors, there is a renewed interest in the vertical-axis turbine concept [1, 2, 3]. Also referred to as cross-flow turbines, vertical-axis turbines provide numerous advantages over traditional horizontal-axis turbines [4]. For example, vertical-axis turbines are not affected by the orientation of the incoming flow, and thus, they do not require complex yaw control mechanisms. This feature is particularly interesting since studies have shown that the yaw control mechanism is one of the components with the largest rate of failure for horizontal-axis turbines operating in wind farms [5, 6, 7]. Another interesting advantage is that the energy extraction plane is rectangular, unlike that of the horizontal-axis turbine. This allows for a better energy resource exploitation potential in the marine context, especially in shallow waters. Moreover, because of their footprint and wake topology, it has been suggested that using vertical-axis turbines could significantly improve the power density of turbine farms [8, 9, 10, 11, 12].

These advantages are obviously very attractive, but the major drawback of vertical-axis turbines is that their efficiency is typically smaller than that of horizontal-axis turbines [13]. Therefore, one of the main objectives in the development of those turbines is to find simple ways of increasing their efficiency.

In this context, the impact of several design parameters have been extensively studied in the literature. For example, many papers have shown the impact of the solidity and of the number of blades on the turbine efficiency [14, 15, 16]. Other studies have also been devoted to the turbine wake, in order to gain a fundamental understanding of the main physical mechanisms affecting the wake recovery rate [17, 18, 19, 20, 21, 22, 23].

However, very little has been published regarding the impact of how the blades are attached to the central shaft of the turbine, despite the accepted fact that the blade support structures can significantly affect the turbine efficiency. Indeed, since the blade support structures (or the struts) are moving with the blades, they generate an additional viscous drag component that results in a negative torque contribution at the turbine shaft. The importance of this negative torque contribution mostly depends on the cross-section shape of the struts. Studies have shown that streamlined struts

[1] thierry.villeneuve.2@ulaval.ca

with low drag are obviously much less detrimental to the turbine efficiency than non-streamlined struts [24, 25, 26]. Bachant et al. [27] even replaced streamlined struts with cylindrical ones to show that when the drag associated with the struts is important, the turbine efficiency may become negative for all operating points. Note that when streamlined struts were used on their turbine, the efficiency value was about 35% at the optimal tip speed ratio.

In addition to the drag component associated with the struts, the lift and the drag on the turbine blades are also affected by the presence of the struts. Therefore, it is expected that the turbine efficiency may be sensitive to the position of the struts. In fact, studies have shown that the efficiency of a given turbine is larger if the struts are located at the tips of the turbine blades, rather than at the mid-span or at other intermediate positions along the blade span [24, 25, 28]. Indeed, struts located at the blade tips can mitigate the tip losses by acting as end-plates or winglets, which are known to have a positive impact on the blade lift and drag coefficients [14, 29, 30].

Therefore, we know that streamlined struts located at the blade tips are less detrimental to the turbine efficiency than non-streamlined struts or than struts located at intermediate positions along the span of the blades, but further work needs to be done in order to improve the design of the blade support structures. In this paper, three-dimensional Unsteady Reynolds-Averaged Navier-Stokes (URANS) simulations are carried out to investigate the impact of the struts on the performance of vertical-axis turbines. In accordance with what is reported in the literature, the impact of the position of the struts is presented to highlight the importance of the blade-strut interference affecting the turbine efficiency. Moreover, the use of inclined struts is investigated in order to assess their potential at improving the performance of vertical-axis turbines and the impact of the junction geometry between the struts and the blades is also presented and analyzed. It is important to note that the objective of this paper is not to optimize a particular vertical-axis turbine, but rather to provide insights about the physics at play and to draw general conclusions about the design of the blade support structures for vertical-axis turbines.

In Section 2, the numerical methodology used in this work is presented. Then, the impact of the position of the struts and of the use of inclined struts is analyzed in Sections 3.1 and 3.2. The importance of the geometry of the blade-strut junctions is later presented in Section 3.3. Finally, the effect of the tip speed ratio on the turbine efficiency is assessed in Section 4, and the results are further interpreted and discussed in Section 5.

2. Methodology

2.1. Turbine description

Without loss of generality, single-blade H-Darrieus vertical-axis turbines are considered here [31]. Figure 1 shows a schematic representation of the hypothetical turbine without strut that is used as a reference case throughout this paper. Note that this reference turbine is the same as the one simulated by some of the authors in a previous work [32].

The straight and rectangular turbine blade is formed with a NACA 0015 cross-section profile having a chord length c. The turbine diameter, D, is $7\,c$ and the solidity is thus $\sigma = (N\,c)/D = 1/7 \simeq 0.143$, with N being the number of blades ($N = 1$ here). The aspect ratio of the turbine is $b/c = 7.5$.

The attach point of the blade is located one-third of the chord length behind the leading edge ($x_p = c/3$). At the angular position $\theta = 0°$, the attach point of the blade is located at the uppermost position in the y direction (see Figure 1).

The turbine tip speed ratio is defined as $\lambda = (\Omega R)/U_\infty$, where U_∞ is the freestream velocity, Ω is the angular velocity of the turbine and $R = D/2$. For all the simulations presented in Section 3, the turbine operates at a tip speed ratio of $\lambda = 3.25$ which corresponds to an optimal operating point based on two-dimensional numerical simulations (see Section 4). The sensitivity of the turbine efficiency on the tip speed ratio is also assessed in Section 4. Note that the turbine here operates in a steady and uniform incoming flow.

The global Reynolds number based on the turbine diameter and on the freestream velocity is set to $Re_D = (U_\infty D)/\nu = 1.0 \times 10^7$, where ν is the kinematic viscosity of the fluid. The Reynolds number based on the chord length of the blade and following the definition proposed by Miller et al. [33, 34] is obtained as:

$$Re_c = \frac{U_\infty\, c\, (1+\lambda)}{\nu} \simeq 6.1 \times 10^6 \ . \qquad (1)$$

At such a high value, the results are assumed to be essentially independent of the Reynolds number [33, 34, 35, 36].

Various strut configurations are investigated in this paper and the different geometries are presented in Section 3. It is important to note that all the struts that are used have the same profile and the same chord length as the turbine

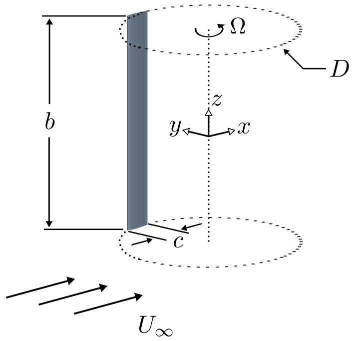

Figure 1: Schematic representation of the geometry of the reference turbine without strut, with the definition of some geometric parameters. Note that the position of the blade in this figure corresponds to the angular position $\theta = 0°$.

blade. Also, when struts are present, the dimensions of the turbine are exactly the same as the reference turbine without strut, i.e., the chord length of the blade (c), the turbine diameter (D) and the span (b) remain unchanged.

2.2. *Efficiency and power coefficient*

The turbine efficiency (η), or the mean power coefficient ($\overline{C_P}$), can be decomposed in two contributions: the contribution associated with the mean (i.e., averaged over one complete turbine revolution) power coefficient on the blade ($\overline{C}_{P,blade}$) and the contribution associated with the mean power coefficient on the struts ($\overline{C}_{P,struts}$). The sum of these two contributions is equal to the overall turbine efficiency:

$$\begin{aligned} \eta \ = \ \overline{C_P} \ &= \ \overline{C}_{P,blade} + \overline{C}_{P,struts} \\ &= \frac{1}{2\pi} \int_0^{2\pi} \Big(C_{P,blade}(\theta) + C_{P,struts}(\theta) \Big) \, \mathrm{d}\theta \, . \end{aligned} \tag{2}$$

The instantaneous power coefficients associated with the blade and the struts ($C_{P,blade}(\theta)$ and $C_{P,struts}(\theta)$) are computed using the following relations:

$$C_{P,blade}(\theta) \ = \ \frac{T_{blade}(\theta)\,\Omega}{0.5\,\rho U_\infty^3 bD} \, , \tag{3}$$

$$C_{P,struts}(\theta) \ = \ \frac{T_{struts}(\theta)\,\Omega}{0.5\,\rho U_\infty^3 bD} \, , \tag{4}$$

where ρ is the density of the fluid, and $T_{blade}(\theta)$ and $T_{struts}(\theta)$ respectively are the instantaneous torque generated by the blade and the struts about the turbine axis of rotation.

2.3. *Numerical methodology*

The numerical simulations are carried out with the finite-volume Navier-Stokes solver Siemens® STAR-CCM+® [37]. Second order schemes are used for the convective and diffusive fluxes as well as for the temporal discretization. The flow is considered to be incompressible. For the pressure-velocity coupling, a segregated approach with the SIMPLE (Semi-Implicit Method for Pressure Linked Equations) algorithm is adopted. In the simulations, an Unsteady Reynolds-Averaged Navier-Stokes (URANS) methodology is used with the one-equation Spalart-Allmaras turbulence model with rotation-curvature correction [38, 39, 40].

Figure 2 shows the computational domain and the boundary conditions used in the simulations. The inlet boundary condition is located $15D$ upstream of the turbine, where a uniform velocity U_∞ is imposed with a turbulent viscosity ratio of $\nu_t/\nu = 0.2$, as recommended by Spalart and Rumsey [41]. A uniform reference static pressure (set to zero) is imposed at the outlet boundary, that is located $30D$ downstream of the turbine. The four lateral boundaries of the domain are symmetry planes. As shown in Figure 2, only one-half of the turbine is simulated, since a symmetry

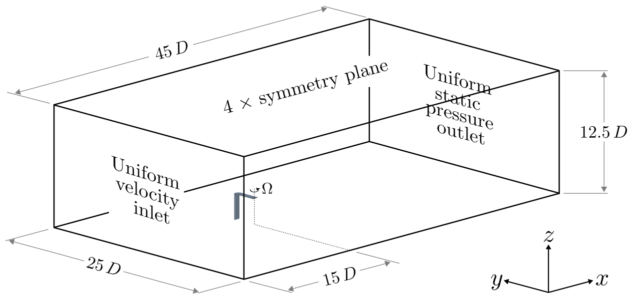

Figure 2: Schematic representation of the computational domain and the boundary conditions used in the simulations. The turbine configuration illustrated in the domain is the turbine with the tip struts (see Figure 7d). Note that the turbine is scaled up by a factor of 5 for clarity and that only the upper half is seen through the bottom symmetry plane. The blockage ratio is 0.17%.

plane is used at the mid-span of the turbine blade ($z/b = 0$). Therefore, for a turbine with tip struts for example (see Figure 7d), only one strut and half the span of the blade are simulated. This choice is made in order to reduce the computational costs of the simulations. Note that the turbine axis of rotation is centered in the computational domain in the transverse direction (y direction). Given the blockage ratio of 0.17%, the lateral boundaries of the domain are located far enough from the turbine to ensure an almost unconfined environment [42]. A uniform velocity and turbulent viscosity ratio having the inlet boundary condition values and the reference static pressure are imposed throughout the domain as the initial condition (at $t = 0$).

An overset mesh technique is used to allow the rotation of the turbine. A mesh is made for the background region (the computational domain shown in Figure 2) and another one is made for the rotating turbine (the blade and the struts). Figure 3 shows an illustration of the mesh used in a simulation. The configuration illustrated corresponds to the turbine with tip struts ($\phi = 90°$) having rounded blade-strut junctions at a curvature radius $R'/c = 0.5$ (see Figure 14a). Note that *Plane A* in Figure 3a corresponds to the bottom symmetry plane boundary illustrated in Figure 2.

The background mesh (black lines in Figure 3) is made from orthogonal cells. In the region close to the turbine, the cells in the background mesh have dimensions of $\delta_x = \delta_y = 0.03c$, and $\delta_z = 0.06c$. However, in the region swept by the rotation of the strut, the cells are isotropic ($\delta_x = \delta_y = \delta_z = 0.03c$). Since the turbine wake is not investigated in this paper, the mesh resolution is kept relatively fine only up to $4D$ downstream of the turbine, before becoming coarser. Globally, the background mesh is composed of approximately 10 million cells.

The overset mesh region containing the blade and the strut is represented in blue in Figure 3. The meshes were created with great care and we paid particular attention to cell quality and other mesh considerations. The overset mesh is composed of polyhedral cells and the prism layer near the no-slip walls ensures that the dimensionless normal wall distance (y^+) of all the cells in contact with the surface of the turbine remains close to 1 and that the maximum growth factor does not exceed 1.2. The cross-section profiles of the blade and the strut are each composed of 400 nodes. The central region of the blade and the strut is made from an extrusion of the blade-strut junction and from an extrusion of the tip region of the strut (see Figures 3c and 3d). The resolution at the exterior of the overset mesh is chosen to match that of the background mesh to ensure a smooth interpolation between these two meshes. Depending on the strut configuration, the blade-strut overset mesh is composed of between 20 and 35 million cells.

For the turbine whose mesh is illustrated in Figure 3, Figure 4 provides a contour of the y^+ values on the surface of the turbine and a graph of the y^+ values along the chord length of the blade at the mid-span plane of the turbine ($z = 0$) at the angular position $\theta = 90°$. It is indeed around the angular position $\theta = 90°$ that the largest values of y^+ are reached on the surface of the blade during a turbine revolution. However, as can be seen in Figure 4, even at $\theta = 90°$, the y^+ values do not exceed 1.5 anywhere on the turbine.

In the simulations, the temporal integration is such that each turbine revolution (complete blade rotation) is divided into 1000 time steps. At every time step, the residuals must decrease by three orders of magnitude and the difference in the power coefficient associated with the blade ($C_{P,blade}$) must not exceed 5×10^{-6} between successive iterations. These criteria result in approximately 50 iterations per time step. The efficiency values reported in Section 3 for the different turbine configurations are computed approximately 25 turbine revolutions after the beginning of the simulations, when the flow has become statistically stationary.

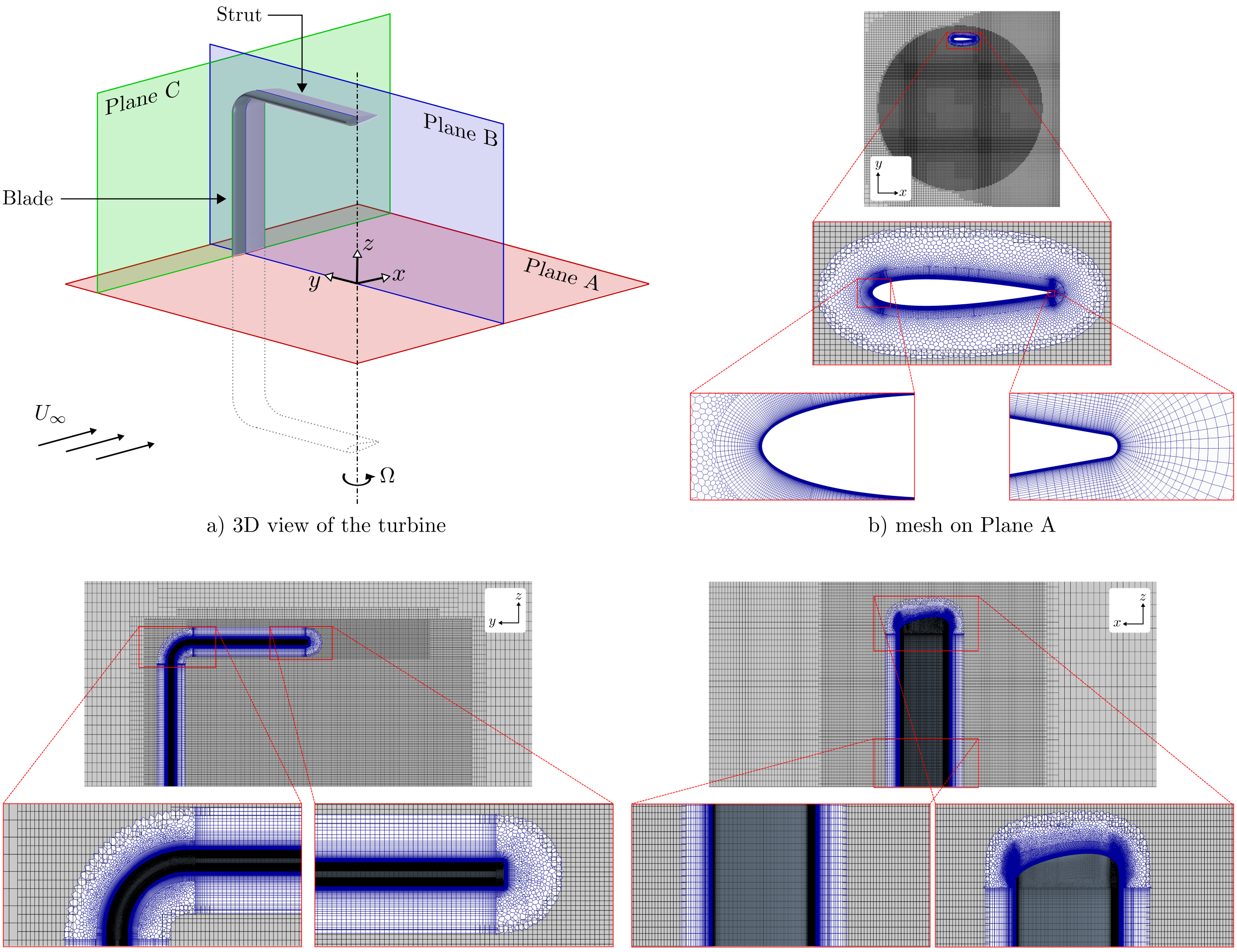

a) 3D view of the turbine

b) mesh on Plane A

c) mesh on Plane B

d) mesh on Plane C

Figure 3: Illustration of the background mesh (black lines) and the overset mesh (blue lines) on multiple plane sections for the turbine with tip struts ($\phi = 90°$) having rounded blade-strut junctions at a curvature radius $R'/c = 0.5$ (the turbine configuration presented in Figure 14a). Note that *Plane A* is a symmetry plane boundary in the computational domain (see Figure 2).

2.4. Validation

In order to ensure the validity of the URANS methodology and the meshing technique used in the present study, the problem investigated experimentally by Chow et al. [43, 44] has been simulated. In their experiment, the pressure coefficients on the surface of a lifting wing made of a NACA 0012 profile with a rounded tip have been measured at different spanwise locations at a Reynolds number of $Re = U_\infty c/\nu = 4.6 \times 10^6$.

In this validation simulation, the turbulence model, the meshing technique and the cell size are the same as what is used in this study, as presented in Section 2.3. However, the wing geometry, the size of the computational domain and the Reynolds number are adjusted to match the case studied by Chow et al. Note that care has been taken to match the measured experimental velocity (U/U_{ref}) at the probe location reported by Churchfield and Blaisdell [45, 46].

Figure 5 shows the experimental pressure coefficient values (C_p) reported by Chow et al. [43] (black markers) as well as the results obtained with the present numerical methodology (red curves) at three spanwise positions. At $z/b = 0.362$, the numerical curve and the experimental data are almost superimposed along the entire chord length of the wing. At $z/b = 0.906$ and $z/b = 0.966$, there are small differences on the wing suction side near the trailing edge, but globally, the numerical curves match the experimental data very well. Note that the position $z/b = 0.966$ roughly corresponds to the position of the core of the tip vortex, which explains the presence of the suction peak near

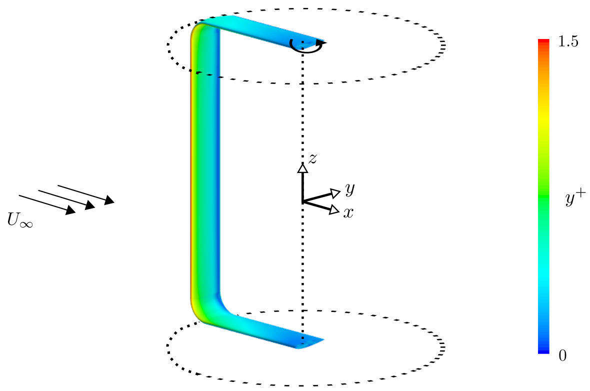

(a) Contour of y^+ values

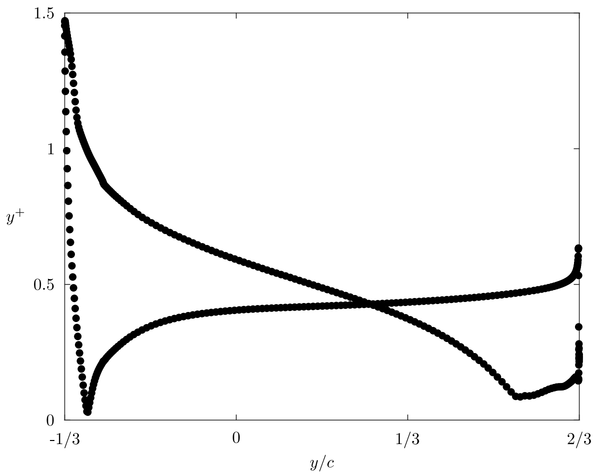

(b) y^+ values along the chord length of the blade at $z = 0$

Figure 4: Contour of y^+ values for the cells that are in contact with the surface of the turbine (a) and distribution of the y^+ values along the chord length of the blade at the mid-span plane of the turbine (b) for the turbine with tip struts ($\phi = 90°$) having rounded blade-strut junctions at a curvature radius $R'/c = 0.5$ (see Figure 14a) at the angular position $\theta = 90°$.

the trailing edge of the wing [43].

For further validation, multiple simulations have also been carried out on a turbine with struts. For the turbine configuration with tip struts ($\phi = 90°$) having rounded blade-strut junctions at a curvature radius $R'/c = 0.5$ (see Figure 14a), simulations have been conducted using smaller time steps and using a finer mesh resolution. Note that this turbine configuration, the mesh of which is shown in Figure 3, is the one leading to the largest efficiency value obtained in this paper. A simulation has thus been conducted using 2000 time steps per turbine revolution (instead of 1000 time steps for the base case) and another simulation has been carried out using a finer spatial resolution in both the background mesh and the overset mesh, leading to a total of 70 million cells (instead of 34 million cells for the base case). Moreover, in order to assess the impact of the turbulence model on the results presented in this paper, another simulation has been conducted using the $k - \omega$ SST turbulence model (instead of the Spalart-Allmaras turbulence model for the base case).

Figure 6 shows the evolution of the instantaneous power coefficient ($C_P = C_{P,blade} + C_{P,struts}$) over one turbine revolution for the base case (black curve), for the case using a finer temporal resolution (blue curve), for the case using a finer spatial resolution (red curve) and for the case using the $k - \omega$ SST turbulence model (green curve). One can conclude that the spatial and temporal resolutions of the base case are appropriate given that there is essentially no difference between the three curves. This is not surprising since a similar resolution had already been shown to be adequate in previous works [19, 32]. We also see that the choice of turbulence model used in the simulation does not

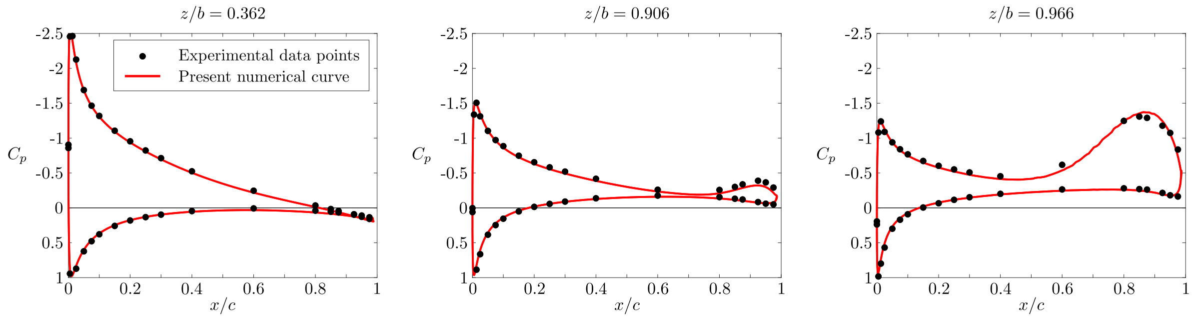

Figure 5: Comparison between the surface pressure coefficient distributions reported by Chow et al. [43] (black markers) and the distributions obtained with the present numerical methodology (red curves) at different spanwise locations.

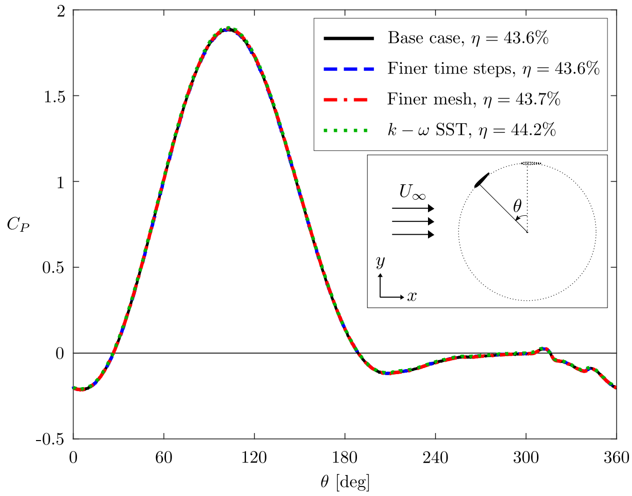

Figure 6: Evolution of the instantaneous power coefficient ($C_P = C_{P,blade} + C_{P,struts}$) over a complete turbine revolution for the turbine with tip struts having rounded blade-strut junctions at a curvature radius $R'/c = 0.5$ (see Figure 14a).

affect the power coefficient curve, and thus the turbine efficiency. This last observation can be explained by the fact that the boundary layers remain attached to the blade for the entire turbine revolution at the tip speed ratio considered. As shown by the authors in a previous study [29], the Spalart-Allmaras and the $k-\omega$ SST turbulence models predict similar force coefficients on the turbine blade for cases with attached boundary layers. Therefore, at high Reynolds numbers, these two turbulence models lead to similar results at the tip speed ratios investigated in this paper.

3. Results

3.1. Position of the struts

At first, in order to evaluate the impact of the position of the struts on the turbine efficiency, the four turbine configurations that are shown in Figure 7 are simulated. Recall that the struts considered throughout this paper have the same profile and the same chord length as the turbine blade. The dimensions of the turbines with struts are the same as those of the reference turbine, i.e., the values of c, b and D remain unchanged. Also, the four turbines illustrated in Figure 7 operate at the same tip speed ratio of $\lambda = 3.25$. For the turbine with the mid-span strut (Figure 7b), the computational domain used is not the one presented in Figure 2. Indeed, for that particular case, no symmetry plane is used at the mid-span of the turbine blade because of the presence of the strut. Instead, a complete turbine is simulated, in a computational domain twice larger in the z direction than that presented in Figure 2.

The global efficiency of the four turbine configurations illustrated in Figure 7 is reported in Table 1, together with the values of $\overline{C_{P,blade}}$ and $\overline{C_{P,struts}}$. The idealized reference turbine without strut (Figures 1 and 7a) has the largest

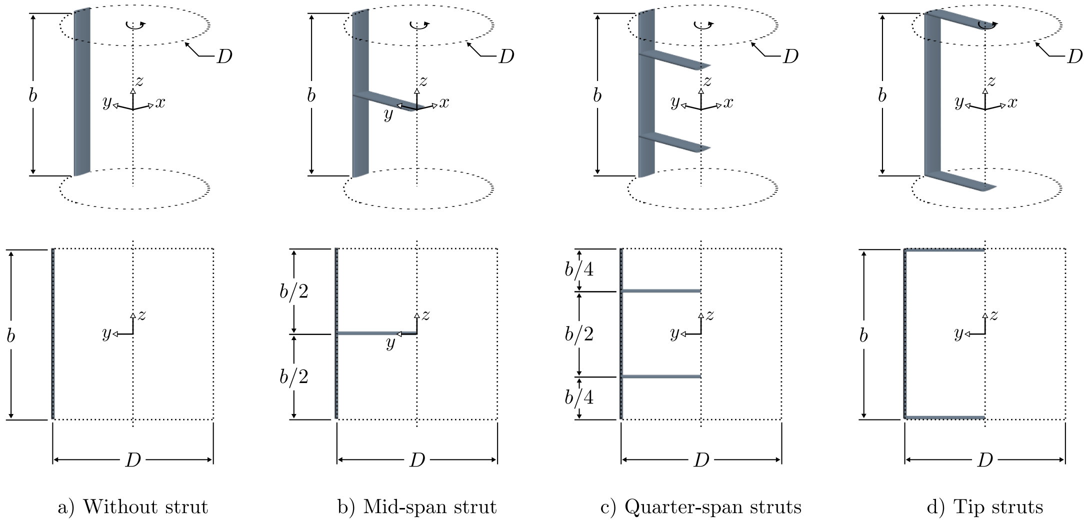

Figure 7: 3D view (top) and front view (bottom) of the geometry of the reference turbine without strut (a), the turbine with the mid-span strut (b), the turbine with quarter-span struts (c) and the turbine with tip struts (d).

efficiency value. For the turbine configuration with the single strut located at the mid-span of the turbine blade (Figure 7b), the efficiency is significantly smaller than for the reference turbine. It is however interesting to note that the negative mean power coefficient associated with the strut is not very large ($\overline{C_{P,\,strut}} = -0.021$). For that case, the low turbine efficiency is mostly due to the loss in the mean power coefficient associated with the blade. Indeed, the power reduction on the blade because of the presence of the strut is more than three times larger than the negative mean power coefficient associated with the strut itself. In other words, for the turbine with the mid-span strut, the negative impact of the strut on the blade is much more important than the actual presence of the strut.

For the turbine with two quarter-span struts (Figure 7c), the efficiency is also significantly smaller than for the reference turbine. Again, it is the decrease in the mean power coefficient associated with the blade that is responsible for most of the difference. Indeed, the mean power coefficient associated with the blade is 37% smaller than for the reference turbine.

For the turbine with two tip struts (Figure 7d), the efficiency is better than for the two other turbines with struts, since the mean power coefficient associated with the blade is closer to that of the reference turbine. Moreover, the negative mean power coefficient associated with the struts is considerably smaller (in absolute value) than for the turbine with the quarter-span struts. Note that the value of $\overline{C_{P,\,struts}}$ is even close to that of the turbine with the mid-span strut, even though there are two struts instead of just one.

Figure 8 shows the evolution of the instantaneous power coefficient ($C_P = C_{P,blade} + C_{P,struts}$, solid lines) and the instantaneous power coefficient associated with the blade only ($C_{P,blade}$, dashed lines) over a complete turbine revolution for the four configurations illustrated in Figure 7. As can be seen, it is in the upstream portion of the blade revolution ($0° \leq \theta \leq 180°$) that the turbine with the mid-span strut (blue curve) and the turbine with the quarter-span

Table 1: Efficiency (η) of the four turbines shown in Figure 7, and values of the mean power coefficient associated with the blade and the struts ($\overline{C_{P,\,blade}}$ and $\overline{C_{P,\,struts}}$).

	η	$\overline{C_{P,\,blade}}$	$\overline{C_{P,\,struts}}$
Without strut (Figure 7a)	36.1%	0.361	-
Mid-span strut (Figure 7b)	27.3%	0.294	-0.021
Quarter-span struts (Figure 7c)	18.4%	0.227	-0.043
Tip struts (Figure 7d)	30.6%	0.331	-0.025

struts (green curve) extract significantly less energy from the flow than the reference turbine (black curve). It is also interesting to see that the turbine with the tip struts (red curve) has larger values of instantaneous power coefficient than the two other turbines with struts in the upstream portion of the turbine revolution. However, for the turbine with tip struts, the power coefficient is smaller than that of the reference turbine, especially between $\theta = 90°$ and $\theta = 180°$.

Table 1 shows that the mean power coefficient associated with the struts is relatively small for the three turbines considered. In Figure 8, one can also see that the instantaneous values of $C_{P,\,struts}$ (the difference between the solid and the dashed curves) also remain relatively small during the entire turbine revolution.

Since the turbine efficiency is mainly affected by the decrease in the power coefficient associated with the blade, it suggests that the struts interfere significantly and negatively with the turbine blade, as previously reported in the literature [25]. More precisely, it implies that the presence of the struts has a significant impact on the flow field and on the forces acting on the turbine blade.

In order to visualize this blade-strut interference, Figure 9 shows the spanwise distribution of the section power coefficient ($C_{P'}(z)$) on the turbine blade for the four turbines illustrated in Figure 7. In Figure 9, the half-span of the turbine blade is sampled at 25 sections that are $0.15c$ apart (such width being much coarser than the mesh used for the simulations). The instantaneous power coefficient at the angular position $\theta = 100°$ (i.e., the angular position roughly corresponding to the largest instantaneous power coefficient) is measured on each of the 25 sections, and this distribution is then mirrored about $z/c = 0$.

The black markers in Figure 9 show the section power coefficient distribution for the reference turbine without strut. As can be seen, the mid-span region of the blade is associated with large values of section power coefficient, while the region near the blade tips does not extract much energy from the flow. Indeed, even at the angular position corresponding to the largest instantaneous power coefficient, the region very near the blade tips has negative values of section power coefficient, highlighting the importance of the tip losses for vertical-axis turbines. A similar trend is also reported by others in the literature [14, 32, 47, 48, 49].

As can be seen by examining the blue and green markers in Figure 9, the power extracted by the blade is importantly decreased around the position of the struts. Indeed, the section power coefficient distributions drop close to zero at the spanwise position of the struts. For the turbine with the mid-span strut, the section-power coefficient on the blade is negatively affected by the presence of the strut between $z/c \approx \pm 1.5$. This spanwise width of approximately $3\,c$ is significantly larger than the thickness of the strut ($0.15\,c$). A similar observation can also be made for the turbine with the quarter-span struts.

In Figure 9, one also sees that the tip struts are much less detrimental to the turbine blade (red markers). Even if the tip struts affect the power extracted by the blade, they impact the blade in a region in which it extracts significantly less energy from the flow. In other words, the tip struts do not ruin the mid-span region of the blade, where most of

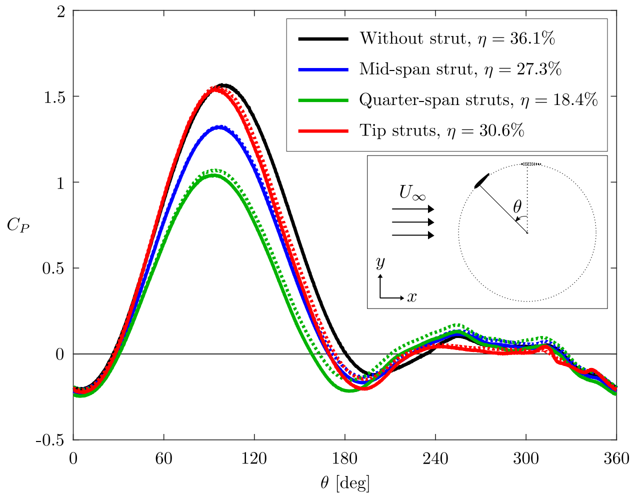

Figure 8: Evolution of the instantaneous power coefficient (solid lines, $C_P = C_{P,\,blade} + C_{P,\,struts}$) and the instantaneous power coefficient associated with the blade (dashed lines, $C_{P,\,blade}$) over a complete blade revolution for the four turbine configurations shown in Figure 7.

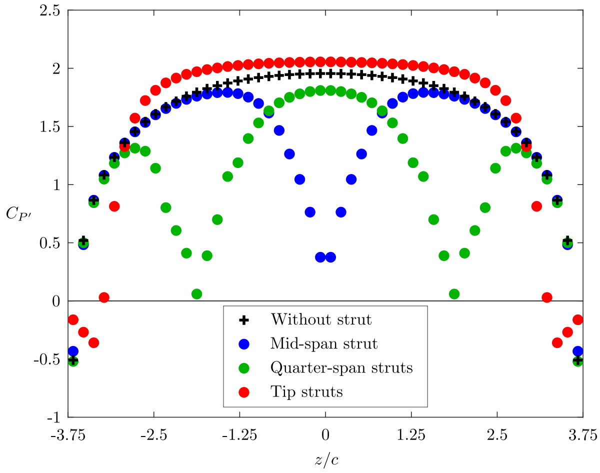

Figure 9: Section power coefficient distribution ($C_{P'}$) along the span of the blade for the four turbines shown in Figure 7, at the angular position $\theta = 100°$.

the energy extraction occurs. The turbine with the tip struts has even larger values of section power coefficient at the mid-span of the blade than the reference turbine. This can be explained by the fact that the tip struts act on the blade in a similar way as winglets or end-plates do for lifting wings [29]. This aspect is discussed in more detail in Section 3.3.

To support the observations made in Figure 9, Figure 10 shows a volume rendering of the magnitude of the vorticity vector around the reference turbine and around the turbine with the mid-span strut. Recall that the vorticity shed by a lifting blade is proportional to the spanwise and temporal variations of the lifting force experienced by the blade. Therefore, the important cross-flow vortices (perpendicular to the direction of the blade) shed on each side of the mid-span strut are related to a decrease in the lift on the turbine blade at this spanwise location. Consequently, if the lift on the blade decreases locally around the junction with the strut, the section power coefficient also decreases, as also seen in Figure 9.

3.2. Inclined struts

A previous study suggested that inclined struts could be beneficial to the efficiency of vertical-axis turbines [50]. The idea is that the important lifting force experienced by the blade in the upstream portion of the turbine revolution ($0° \leq \theta \leq 180°$) is such that the blade extracts energy from the flow, since the positive circumferential component of the lift is larger than the negative component of the drag. Conversely, the drag force experienced by the struts results in a negative torque at the turbine shaft. Thus, it costs energy for the struts to rotate with the blade. So, for turbines with inclined struts, there may be some configurations for which the inclined struts could generate lift, similar to the blade, and extract energy from the flow.

In order to investigate this possibility, turbines with different blade-strut angles (ϕ) have been simulated and the geometries are presented in Figure 11. Since the results from Section 3.1 show that the struts should be located at the blade tips in order to limit their negative impact on the turbine efficiency, only inclined struts positioned at the blade tips are considered here. As shown in Figure 11, turbines with blade-strut angles of $\phi = 80°$, $\phi = 67.5°$ and $\phi = 45°$ have been simulated; the configuration with non-inclined struts ($\phi = 90°$) being the turbine already presented in Section 3.1 (the turbine with tip struts in Figure 7d). The efficiency of these four turbines is reported in Table 2, along with the efficiency of the reference turbine without strut.

As can be seen in Table 2, the use of inclined struts is not beneficial to the turbine efficiency for the configurations tested. Indeed, the turbines with blade-strut angles of $\phi = 80°$, $\phi = 67.5°$ and $\phi = 45°$ are much less interesting in terms of efficiency than the turbine with non-inclined struts ($\phi = 90°$). Again, the decrease in efficiency compared to the reference turbine without strut is mainly related to the loss in the mean power coefficient associated with the blade. The larger the blade-strut angle ϕ, the larger the mean power coefficient associated with the blade, and the larger the turbine efficiency.

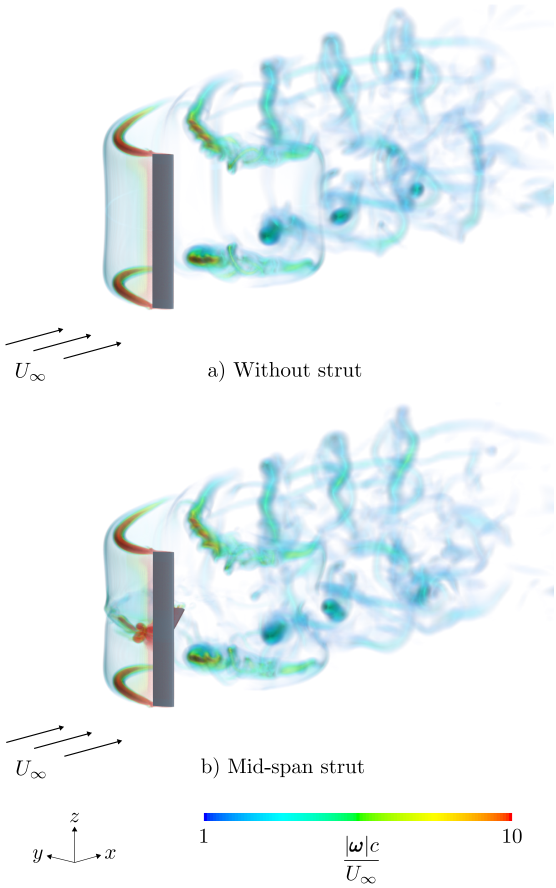

Figure 10: Volume rendering of the magnitude of the vorticity vector around the reference turbine without strut (a) and the turbine with the mid-span strut (b). Note that, for better visualization, the turbine blade is here located at the angular position $\theta = 125°$.

We also note that highly inclined struts can have a positive value of mean power coefficient: the turbine with a blade-strut angle of $\phi = 45°$ has $\overline{C_{P,\,struts}} = 0.014$, confirming that inclined struts can extract some energy from the flow. However, these highly inclined struts interfere importantly with the flow over the turbine blade and, globally, the efficiency of this turbine is 30% smaller than that of the turbine with non-inclined struts ($\phi = 90°$).

Interestingly, if we simulate a "turbine" with a blade-strut angle of $\phi = 45°$, but without the presence of the blade (leaving only the inclined struts to rotate at a tip speed ratio $\lambda = 3.25$), we obtain a value of $\eta = \overline{C_{P,\,struts}} = 0.113$. This value of mean power coefficient is significantly larger than when the blade is added to the turbine ($\overline{C_{P,\,struts}} = 0.014$) and this highlights even further the importance of the blade-strut interactions.

Figure 12 shows the evolution of the instantaneous power coefficient for the turbines shown in Figure 11 and for the reference turbine without strut. As expected, it is in the upstream portion of the blade revolution ($0° \leq \theta \leq 180°$) that the impact of the struts on the power coefficient is the most important. As can be seen in Figure 12, the larger the blade-strut angle ϕ, the larger the instantaneous power coefficient in the upstream portion of the turbine revolution.

For the turbine with a blade-strut angle of $\phi = 45°$, it is also interesting to notice in Figure 12 (green curve) that the instantaneous power coefficient associated with the struts is relatively large in the upstream portion of the blade revolution, while it is mostly negative in the downstream portion. Recall that the difference between the solid curves and the dashed curves in Figure 12 represents the power coefficient associated with the struts.

Figure 13 shows the section power coefficient distribution along the span of the blade for the turbines with inclined struts at the angular position $\theta = 100°$. As can be seen, the inclined struts affect the section power coefficient

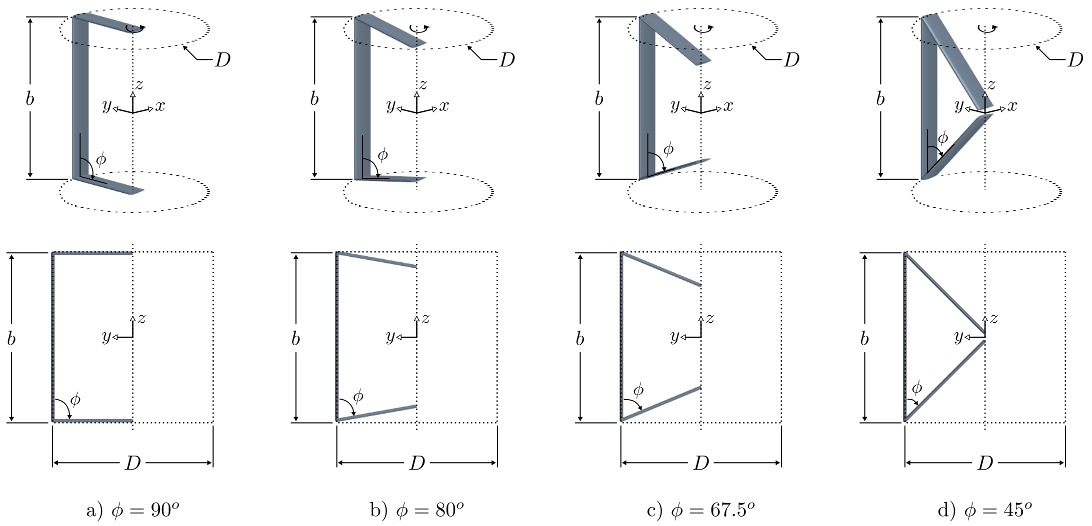

Figure 11: 3D view (top) and front view (bottom) of the geometry of the turbines with different blade-strut angles: $\phi = 90°$ (a), $\phi = 80°$ (b), $\phi = 67.5°$ (c) and $\phi = 45°$ (d).

Table 2: Efficiency (η) of the turbines with inclined struts shown in Figure 11, and values of the mean power coefficient associated with the blade and the struts ($\overline{C_{P,\,blade}}$ and $\overline{C_{P,\,struts}}$).

	η	$\overline{C_{P,\,blade}}$	$\overline{C_{P,\,struts}}$
Without strut (Figure 7a)	36.1%	0.361	-
$\phi = 90°$ (Figures 7d and 11a)	30.6%	0.331	-0.025
$\phi = 80°$ (Figure 11b)	29.2%	0.313	-0.021
$\phi = 67.5°$ (Figure 11c)	28.8%	0.301	-0.013
$\phi = 45°$ (Figure 11d)	21.3%	0.199	0.014

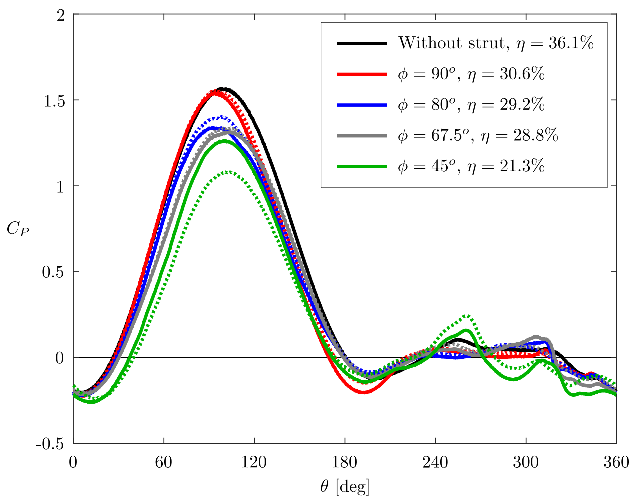

Figure 12: Evolution of the instantaneous power coefficient (solid lines, $C_P = C_{P,\,blade} + C_{P,\,strut}$) and the instantaneous power coefficient associated with the blade (dashed lines, $C_{P,\,blade}$) over a complete blade revolution for the turbine configurations shown in Figure 11.

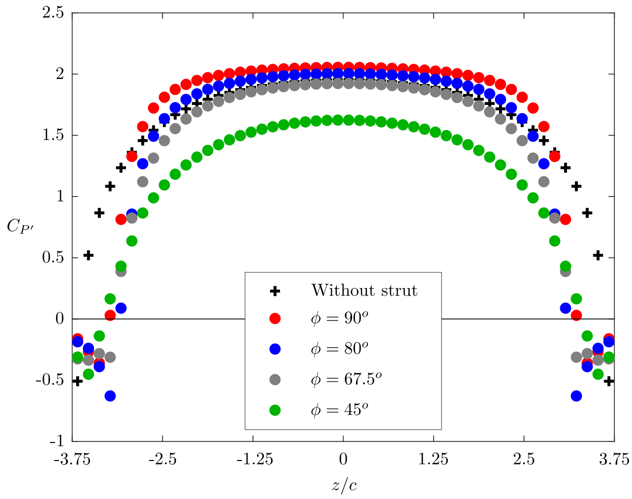

Figure 13: Section power coefficient distribution ($C_{P'}$) along the span of the blade for the turbines shown in Figure 11, at the angular position $\theta = 100°$.

distributions over the entire span of the turbine blade. Again, the larger the blade-strut angle ϕ, the better the section power coefficient distribution.

The results presented in Figure 13 illustrate the importance of the blade-strut interference for turbines with inclined struts. Indeed, even if the struts are located at the blade tips, they can still be highly detrimental to the turbine efficiency. The close proximity between the span of the turbine blade and the struts may explain this important blade-strut interference. For the turbine with a blade-strut angle of $\phi = 45°$, one sees in Figure 11d that the struts and the blade are in relatively close proximity over a large distance on the blade span. This close proximity affects negatively the flow field around the blade, resulting in a turbine blade that extracts significantly less energy from the flow. As the blade-strut angle approaches $\phi = 90°$, the struts and the blade get further apart and the blade-strut interference becomes much less severe.

3.3. Rounded blade-strut junction geometries

In Sections 3.1 and 3.2, only turbines with sharp junctions between the struts and the blade were considered. In the present section, rounded blade-strut junction geometries are used on the turbines, and Figure 14 illustrates some of the configurations simulated. More precisely, for the turbine with non-inclined tip struts ($\phi = 90°$) and for the turbines with blade-strut angles of $\phi = 80°$, $\phi = 67.5°$ and $\phi = 45°$, simulations have been conducted with rounded blade-strut junctions having a curvature radius of $R'/c = 0.5$, $R'/c = 1$, $R'/c = 1.5$ and $R'/c = 2$. Figure 14a shows the geometry of the turbine with non-inclined tip struts ($\phi = 90°$) with the four curvature radii simulated. In Figure 14a, $R'/c = 0$ corresponds to the turbine already presented in Sections 3.1 and 3.2 (see Figures 7d and 11a). Figures 14b, 14c and 14d show some of the configurations simulated for the turbines with inclined struts in order to give a general idea of the geometry of these turbines with rounded blade-strut junctions. As can be seen in Figure 14, the dimensions of the turbines remain unchanged (same values of c, b and D as the reference turbine).

Figure 15 summarizes the results for the turbines with rounded blade-strut junctions. Each marker in Figure 15 is obtained from a three-dimensional numerical simulation. The horizontal black line represents the efficiency of the reference turbine without strut. The four leftmost markers on the graph provide the efficiency of the turbines with sharp blade-strut junctions ($R'/c = 0$), as reported in Section 3.2. The other 16 markers provide the efficiency of the different turbines with rounded blade-strut junctions that have been simulated.

As one can see in Figure 15, the use of rounded blade-strut junctions leads to an important increase in the turbine efficiency. Indeed, the best configuration presented in this paper (the turbine with non-inclined tip struts having rounded blade-strut junctions at a curvature radius $R'/c = 0.5$) has an efficiency of 43.6%. This value is particularly interesting given that the simulations are conducted in an essentially unconfined environment (see Section 2.3) and that the efficiency of the reference turbine without strut is $\eta = 36.1\%$. It corresponds to a relative increase of 21%

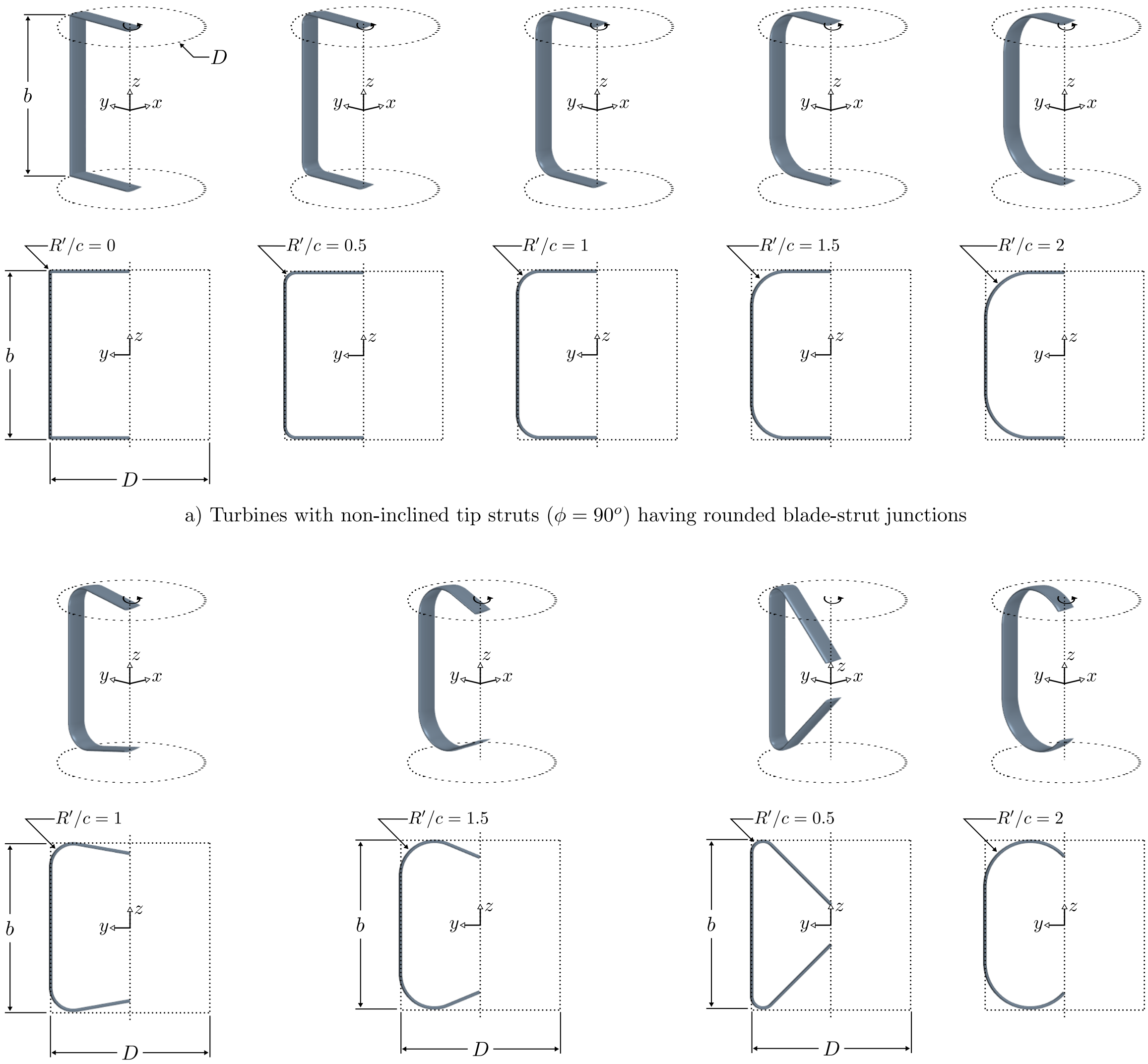

a) Turbines with non-inclined tip struts ($\phi = 90^o$) having rounded blade-strut junctions

b) Turbine with a blade-strut angle of $\phi = 80^o$ and rounded blade-strut junctions

c) Turbine with a blade-strut angle of $\phi = 67.5^o$ and rounded blade-strut junctions

d) Turbines with a blade-strut angle of $\phi = 45^o$ and rounded blade-strut junctions

Figure 14: 3D view (top) and front view (bottom) of the geometry of some of the turbines simulated with rounded blade-strut junctions.

compared to the efficiency of the reference turbine. It is also interesting to note that, even for the turbines with inclined struts, the efficiency value is larger than the reference turbine for most of the curvature radii simulated.

For the turbine with non-inclined tip struts and for the turbine with a blade-strut angle of $\phi = 45°$, Figure 16 shows the evolution of the power coefficient over a complete turbine revolution for the different blade-strut junction curvature radii simulated. As expected, the rounded blade-strut junctions mainly affect the power coefficient in the upstream portion of the turbine revolution ($0° \leq \theta \leq 180°$). For $\phi = 90°$, the larger the power coefficient in the upstream portion of the turbine revolution, the larger the turbine efficiency.

For the turbine with a blade-strut angle of $\phi = 45°$, we also see, in Figure 16b, that the use of a curvature radius as small as $R'/c = 0.5$ already affects significantly the power coefficient curve and the turbine efficiency. Even if it does not constitute a drastic change in the geometry (see Figures 11d and 14d), the efficiency is 62% larger for the turbine with rounded blade-strut junctions. As discussed in Section 3.2, the close proximity between the blade and the struts seems to be detrimental to the turbine efficiency. Thus, for the turbine with a blade-strut angle of $\phi = 45°$, it

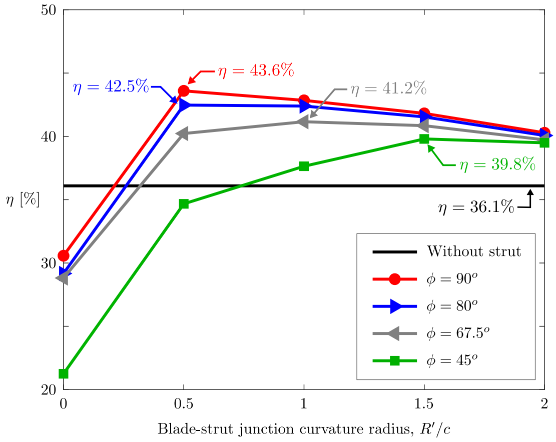

Figure 15: Efficiency (η) of the different turbines simulated with rounded blade-strut junctions. $R'/c = 0$ corresponds to sharp blade-strut junctions.

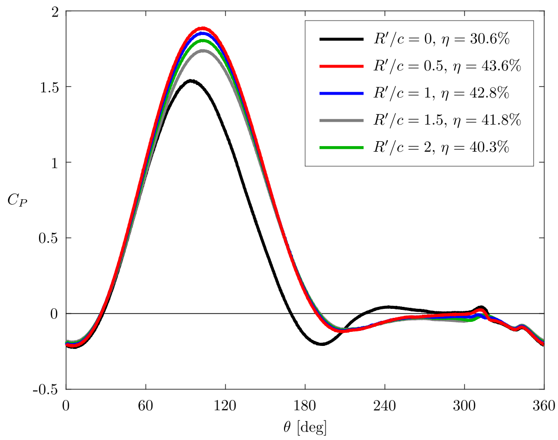

(a) Turbine with non-inclined tip struts ($\phi = 90°$)

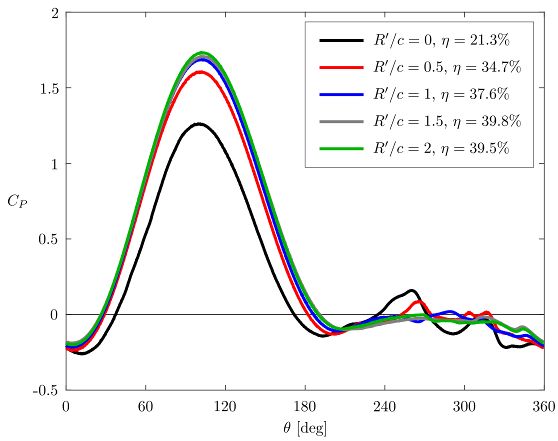

(b) Turbine with a blade-strut angle of $\phi = 45°$

Figure 16: Evolution of the instantaneous power coefficient ($C_P = C_{P,blade} + C_{P,strut}$) over a complete blade revolution for the turbine with non-inclined tip struts ($\phi = 90°$) and for the turbine with a blade-strut angle of $\phi = 45°$ having rounded blade-strut junctions at different curvature radii.

is not surprising that rounded blade-strut junctions are beneficial. The rounded blade-strut junctions allow the struts to be located a little further apart from the blade span (see Figure 14d). Therefore, it is expected that the optimal blade-strut junction curvature radius is larger for the turbine with a blade-strut angle of $\phi = 45°$ than for the turbine with non-inclined tip struts. Indeed, as can be seen in Figure 15, the smaller the blade-strut angle ϕ, the larger the optimal curvature radius.

In order to better understand the effects of the rounded blade-strut junctions on the turbine efficiency, the next analysis mainly focuses on the turbine with non-inclined tip struts ($\phi = 90°$). Table 3 provides the efficiency and the values of $\overline{C_{P,blade}}$ and $\overline{C_{P,struts}}$ for the turbine with tip struts having rounded blade-strut junctions at different curvature radii. Note that $\overline{C_{P,blade}}$ here accounts for the forces acting on the portion of the blade that is parallel to the turbine axis of rotation as well as for the forces acting on the rounded junctions (see Figure 14a). Consequently, $C_{P,struts}$ here accounts exclusively for the part of the geometry that is perpendicular to the rotation axis.

As reported in Table 3, except for the configuration with sharp blade-strut junctions ($R'/c = 0$), the mean power coefficient associated with the struts is positive. Also, one can see that the best turbine efficiency is obtained at $R'/c = 0.5$, which corresponds to the curvature radius leading to the largest value of $\overline{C_{P,blade}}$. As the curvature radius further increases beyond $R'/c = 0.5$, the mean power coefficient associated with the blade decreases. To explain this last observation, one can examine the span of the turbine blade in Figure 14a. As the curvature radius increases, the length of the blade span that is parallel to the turbine axis of rotation decreases. Therefore, it is not surprising to see that the mean power coefficient associated with the blade decreases as the effective span of the blade decreases.

Figure 17 further shows the section power coefficient distribution along the blade span for the turbines with non-inclined tip struts having a curvature radius of $R'/c = 0$, $R'/c = 0.5$ and $R'/c = 2$ at the angular position $\theta = 100°$, as well as for the reference turbine without strut. As can be seen, the turbines with struts have larger values of section power coefficient at the mid-span of the turbine blade than the reference turbine. However, the values of section power coefficient for the turbines with struts differ significantly near the blade tips.

For the turbine with tip struts at $R'/c = 2$ (green markers in Figure 17), the section power coefficient distribution near the blade tips is better than for the reference turbine and for the turbine with sharp blade-strut junctions (black and blue markers respectively). However, the values of section power coefficient are smaller than for the turbine with $R'/c = 0.5$ near the blade tips. As discussed previously, because of the large curvature radius, the effective span of the blade is smaller for the turbine with $R'/c = 2$. It therefore makes sense that it is around the blade tips that the turbine with $R'/c = 0.5$ is better than the turbine with $R'/c = 2$.

To summarize, we know from Figures 15 and 16a that the turbine with non-inclined tip struts having rounded blade-strut junctions at a curvature radius $R'/c = 0.5$ has the best efficiency value of all the configurations simulated; and that it is in the upstream portion of the turbine revolution that its power coefficient is larger than the other turbines. Table 3 shows that the increase in the turbine efficiency is mainly related to the power coefficient associated with the blade. In the upstream portion of the turbine revolution, where the largest angles of attack are reached, the power coefficient associated with the blade is related to the lift and drag coefficients experienced by the blade. Here, for the turbine with $R'/c = 0.5$, Figure 17 shows that the distribution of the section power coefficient is better than for the reference turbine without strut along the entire blade span. Therefore, it suggests that the struts in the turbine with rounded blade-strut junctions at $R'/c = 0.5$ affect positively the lift and the drag on the blade. In other words, one

Table 3: Efficiency (η) and values of the mean power coefficient associated with the blade and the struts ($\overline{C_{P,blade}}$ and $\overline{C_{P,struts}}$) for the turbines with non-inclined tip struts ($\phi = 90°$) having rounded blade-strut junctions (see Figure 14a).

	η	$\overline{C_{P,blade}}$	$\overline{C_{P,struts}}$
Without strut	36.1%	0.361	-
$R'/c = 0$	30.6%	0.331	-0.025
$R'/c = 0.5$	43.6%	0.420	0.016
$R'/c = 1$	42.8%	0.417	0.011
$R'/c = 1.5$	41.8%	0.411	0.007
$R'/c = 2$	40.3%	0.399	0.004

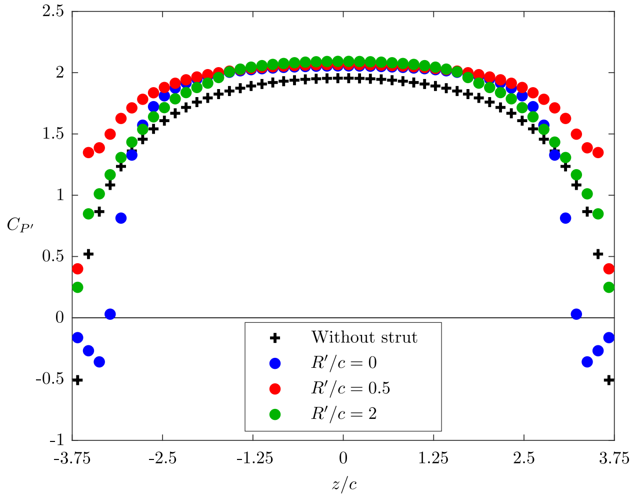

Figure 17: Section power coefficient distribution ($C_{P'}$) along the span of the blade, at the angular position $\theta = 100°$, for the turbines with non-inclined tip struts ($\phi = 90°$) having rounded blade-strut junctions at different curvature radii (see Figure 14a).

may say that the struts with rounded junctions act as efficient winglets, or efficient end-plates, for the turbine blade.

In order to investigate the impact of the struts with rounded junctions on the lift and drag coefficients experienced by the turbine blade, more simulations have been conducted. More precisely, turbine blades with added "winglets" have been simulated and Figure 18 shows the geometries investigated. As can be seen in Figures 18b, 18c and 18d, for rounded junctions at a curvature radius $R'/c = 0.5$, turbines with winglets extending $0.5\,c$, $1\,c$ and $1.5\,c$ are considered. Note that the winglets are all similar to the struts in the turbine with non-inclined tip struts having rounded blade-strut junctions at a curvature radius $R'/c = 0.5$ (see Figures 14a and 18e), except that the winglets do not reach the turbine axis of rotation.

To compare the lift and drag coefficients for the blades with winglets, the circulation and the cross-flow kinetic energy of the vortical wake formed just behind the blade are analyzed. In order to do so, measurements have been made when the turbine blade is located at the angular position $\theta = 90°$ (close enough to the angular position corresponding to the maximum instantaneous power coefficient). The cross-flow vorticity field is analyzed on a plane section that is perpendicular to the y axis (i.e., perpendicular to the motion of the blade at $\theta = 90°$) and that is located $0.1\,c$ behind the trailing edge of the blade. Figure 19 shows the cross-flow vorticity field on the plane section considered for the five turbines illustrated in Figure 18.

For a blade with or without winglets, the lift L exerted by the flow on the blade is equal to the linear impulse I (i.e., the momentum) imparted by the blade to the near-wake vortical flow. Using the half-plane and the mirror image in Figure 19, it is computed as [51]:

$$I = \Gamma_0\, b_0 = \iint \omega_y(x,z)\, z\; dx\, dz\;, \tag{5}$$

where $\omega_y(x,z)$ is the cross-flow vorticity of the near-wake, i.e., the component of the vorticity vector perpendicular to the plane section shown in Figure 19.

The total circulation of the vorticity field for the upper half-plane, Γ_0, can also be computed as:

$$\Gamma_0 = \iint_{z>0} \omega_y(x,z)\; dx\, dz\;. \tag{6}$$

The dimensionless values are then defined using the blade velocity ($\Omega\, R$) and the blade span (b): $I^* = \Gamma_0^*\, b_0^* = \Gamma_0\, b_0/(\Omega\, R\, b^2)$ and $\Gamma_0^* = \Gamma_0/(\Omega\, R\, b)$.

The drag on each blade section or winglet section has two components: the "parasitic drag" (D_p) which basically corresponds to the airfoil friction drag and pressure drag (as in a 2D flow), and the "induced drag" (D_i) which is the

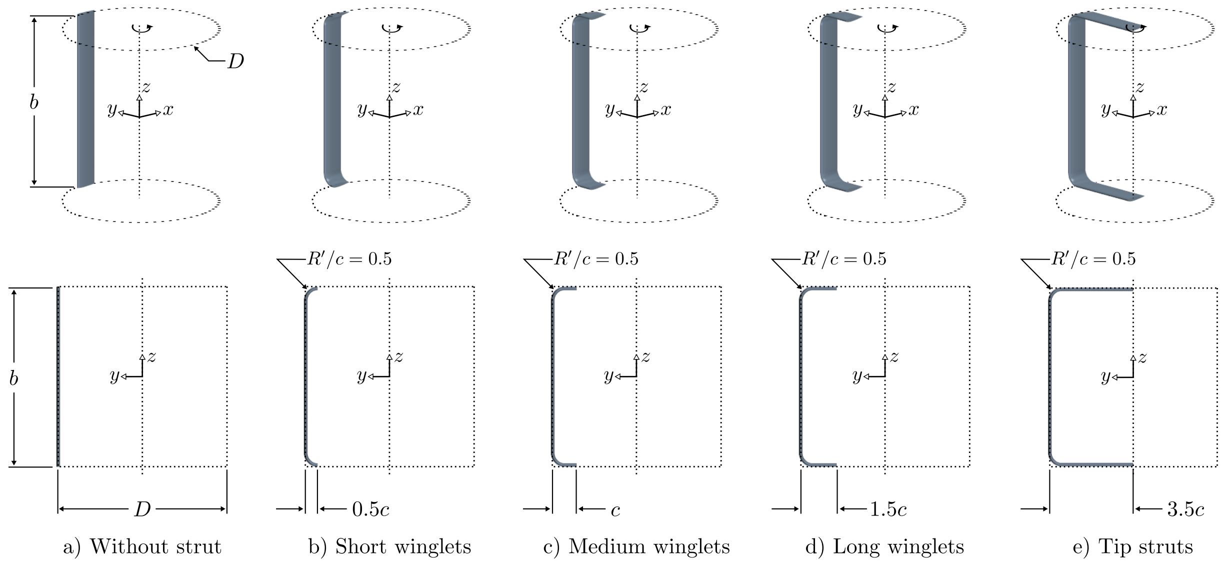

Figure 18: 3D view (top) and front view (bottom) of the geometry of the reference turbine without strut (a), the turbines with the different winglets having rounded junctions at a curvature radius $R'/c = 0.5$ (b, c and d) and the turbine with tip struts ($\phi = 90°$) having rounded blade-strut junctions at a curvature radius $R'/c = 0.5$ (e).

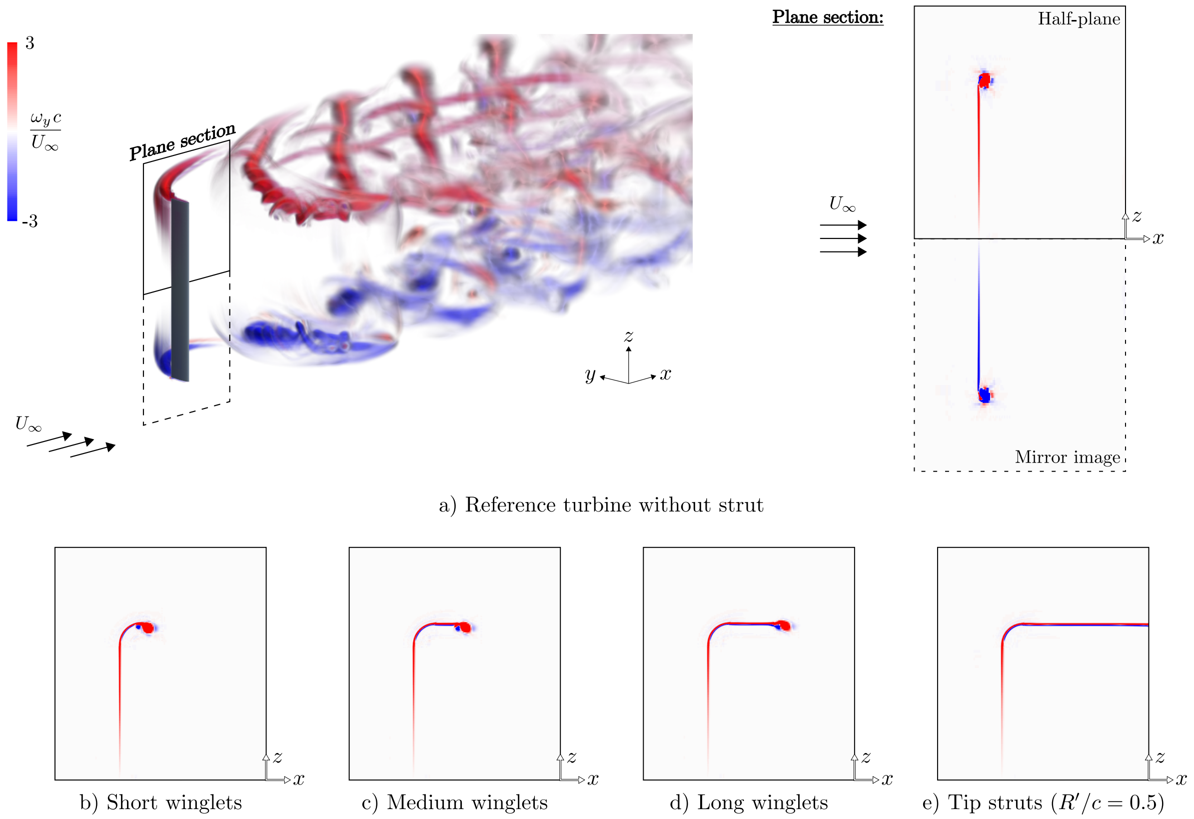

Figure 19: Transverse component of the vorticity vector (ω_y) on a plane section that is perpendicular to the y axis (perpendicular to the motion of the blade at the angular position $\theta = 90°$) and that is located 0.1 c behind the trailing edge of the blade, for the turbines illustrated in Figure 18.

additional drag penalty associated with the fact that a significant vortical wake is shed due to the finite span of the blade, as seen in Figure 19.

If we solely consider the blade without winglet and the blade with short winglets (see Figure 18), we can consider the blade as a wing flying in a uniform flow at a velocity of the order of ΩR. Of course, this is an approximation, but we assume that the results can be useful for relative comparisons.

Thus, we can estimate the induced drag from the kinetic energy, E, of the near-wake cross-flow [52, 53, 54, 55]:

$$\frac{D_i}{\rho} \simeq E \simeq \frac{1}{2} \iint \left(u^2 + w^2\right) \, dx \, dz \, , \tag{7}$$

where (u, w) is the cross-flow velocity induced by the near-wake vorticity ω_y on an unbounded cross-plane.

In Equation (7), the integral can be evaluated efficiently using integration by parts to obtain [51, 56, 57, 58]:

$$E \simeq \frac{1}{2} \iint \psi_y \, \omega_y \, dx \, dz \, , \tag{8}$$

where ψ_y is the stream function, which is the solution of the Poisson equation $\nabla^2 \psi_y = -\omega_y$ in the unbounded cross-plane (Biot-Savart) [58, 59]. Thus, it is obtained as:

$$\psi_y(x, z) = -\frac{1}{4\pi} \iint \ln \left[\frac{(x - x')^2 + (z - z')^2}{b^2} \right] \omega_y(x', z') \, dx' dz' \ . \tag{9}$$

The dimensionless form of the energy estimate is $E^* = E/(\Omega R \, b)^2$.

Since the flow is here turbulent, and since we only have a RANS solution, we can only compute the kinetic energy of the RANS cross-flow field, i.e., the integral of $\frac{1}{2}\left(U^2 + W^2\right)$ where $U = \overline{u}$ and $W = \overline{w}$ are the RANS solutions. By doing so, we don't capture the whole kinetic energy. Nevertheless, we capture a large fraction of it, and we assume that this is sufficient to support the discussion below as we only perform relative comparisons.

In summary, the lift coefficient C_L is proportional to the dimensionless impulse of the near-wake I^*, and the induced drag coefficient C_{D_i} is proportional to the dimensionless energy estimate E^*.

We stress that the turbine with tip struts in Figure 19e is clearly to be excluded from the above analysis. Only the blades with winglets can be considered. Indeed, the above simplified analysis is acceptable for the blade without winglet and for the blade with short winglets in Figure 19b. It is already less acceptable for the blade with medium winglets and clearly not acceptable for the case of the blade with long winglets (since the blade and the winglets do not face a uniform velocity ΩR). The values reported for this last case are thus put in parentheses and must be considered with great caution.

Table 4 provides the dimensionless results obtained for all cases. As can be seen, adding short winglets to the turbine blade leads to an increased value of instantaneous power coefficient at the angular position $\theta = 90°$, and to an improved turbine efficiency. Also, as the length of the winglets increases, $C_P(\theta = 90°)$ and η further increase. Recall that the turbine with tip struts at a curvature radius $R'/c = 0.5$ has the largest values of efficiency and $C_P(\theta = 90°)$.

Compared to the blade without winglet (i.e., the reference turbine without strut), we see that the blade with short winglets and the blade with medium winglets have roughly the same values of I^*, and thus, roughly the same lift. They also have approximately the same values of Γ_0^*. However, what is most notable is that the energy estimate E^* decreases significantly when winglets are added to the turbine blade (e.g., compare the case without winglet to the case with short winglets). Moreover, the values of E^* decrease further when the length of the winglets is increased, as can be seen by comparing the case with short winglets and the case with medium winglets (even if the value of E^* is more disputable for this case).

Therefore, the results of this simplified analysis suggest that the main reason why the instantaneous power coefficient (and the turbine efficiency) is larger for the turbines with winglets than for the turbine without winglet is that the winglets indeed contribute to decrease the induced drag on the blade. Even though the numerical value of the energy estimate for the case with long winglets cannot be trusted blindly, the trend is likely correct, and the induced drag is likely even less.

In summary, the results presented in this section show that using rounded blade-strut junctions is highly beneficial to the efficiency of the vertical-axis turbine considered. It allows to reach efficiency values that are significantly larger than for the reference turbine without strut. Moreover, the simplified analysis done using a blade with rounded

Table 4: Efficiency (η), instantaneous power coefficient (C_P) at $\theta = 90°$ and values of dimensionless impulse ($I^* = \Gamma_0^* b_0^*$), circulation (Γ_0^*), and kinetic energy (E^*) for the blade without winglet (i.e., the reference turbine without strut), the turbine with non-inclined tip struts ($\phi = 90°$) having rounded blade-strut junctions at a curvature radius $R'/c = 0.5$ and the turbines with winglets illustrated in Figure 18.

	η	$C_P(\theta{=}90°)$	I^*	Γ_0^*	E^*
Blade without winglet	36.1%	1.53	0.135	0.146	0.0114
Blade with short winglets	38.3%	1.61	0.134	0.146	0.0108
Blade with medium winglets	41.2%	1.72	0.133	0.142	0.00901
Blade with long winglets	42.7%	1.78	(0.125)	(0.132)	(0.00705)
Blade with struts	43.6%	1.80	-	-	-

winglets suggests that using rounded blade-strut junctions allows to significantly decrease the induced drag on the turbine blade, and thus, allows to increase the turbine efficiency.

4. Effect of the tip speed ratio

For all the simulations presented in this paper, the turbine operates at a tip speed ratio of $\lambda = 3.25$ (see Section 2.1). In Figure 20, in order to discuss the sensitivity of the turbine performance on the operating point, we show the efficiency, at different values of tip speed ratio, of the reference turbine without strut and of the turbine with non-inclined tip struts having rounded blade-strut junctions at a curvature radius $R'/c = 0.5$. We also show the efficiency of a hypothetical two-dimensional turbine (obtained using 2D simulations).

Indeed, the blue curve in Figure 20 reports the efficiency of a 2D turbine ($b/c = \infty$) having all other geometric and operational parameters similar to those presented in Section 2.1. As can be seen, the optimal operating point of this 2D turbine is $\lambda = 3.25$. However, note that this optimum is rather flat: the turbine efficiency does not vary much between $\lambda = 3.0$ and $\lambda = 3.5$.

For the reference turbine without strut, one can see in Figure 20 that the turbine mean power coefficient is slightly larger at $\lambda = 2.75$ than at $\lambda = 3.25$. This suggests that the blade aspect ratio affects the optimal tip speed ratio of the turbine. Indeed, the largest efficiency is obtained at the tip speed ratio for which the blade lift to drag ratio is optimal for the turbine considered. Since the lift and the drag experienced by the blade during a revolution depend on the aspect ratio, it is expected that the optimal tip speed ratio of a turbine of aspect ratio $b/c = 7.5$ is not the same as that of a 2D turbine (of aspect ratio $b/c = \infty$). Nevertheless, for the reference turbine without strut, the difference in efficiency between $\lambda = 2.75$ and $\lambda = 3.25$ is not very significant ($\eta = 37.3\%$ at $\lambda = 2.75$ and $\eta = 36.1\%$ at $\lambda = 3.25$).

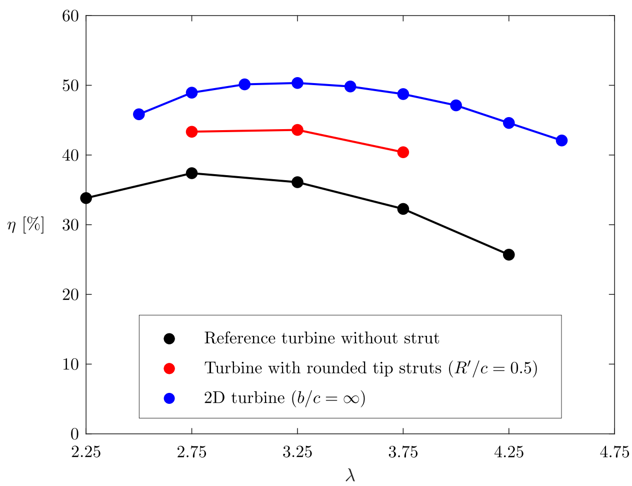

Figure 20: Efficiency of the reference turbine without strut, of the turbine with non-inclined tip struts ($\phi = 90°$) having rounded blade-strut junctions at a curvature radius $R'/c = 0.5$ and of a hypothetical 2D turbine ($b/c = \infty$) at different values of tip speed ratio.

On the other hand, what is interesting to note in Figure 20 is that the efficiency of the optimal turbine simulated in this paper (that with non-inclined tip struts having rounded blade-strut junctions at a curvature radius $R'/c = 0.5$) remains quite large for the three values of tip speed ratio simulated. For this turbine, the optimum is at $\lambda = 3.25$ and the performance curve is quite flat ($\eta = 43.4\%$ at $\lambda = 2.75$, $\eta = 43.6\%$ at $\lambda = 3.25$ and $\eta = 40.4\%$ at $\lambda = 3.75$). This behavior is similar to that of the 2D turbine and this further highlights the benefits of the rounded tip struts: indeed they help to obtain a flow that is essentially two-dimensional over a significant portion of the blade and they also help to reduce the drag. Consequently, when rounded tip struts are used, the efficiency of the 3D turbine becomes closer to that of a hypothetical 2D turbine.

5. Additional discussion

In this paper, we have shown that using tip struts with rounded blade-strut junctions can lead to very interesting efficiency values for the vertical-axis turbine considered, and especially for the case with non-inclined struts ($\phi = 90°$). However, only turbines with blade-strut angles between $\phi = 45°$ and $\phi = 90°$ have been discussed so far.

Turbines with blade-strut angles up to $\phi = 135°$ have also been simulated, but their efficiency is smaller than most of the cases presented in Section 3. Indeed, for the turbines with blade-strut angles of $\phi > 90°$, even if the mean power coefficient associated with the struts is better than for the configurations with $\phi \leq 90°$, the power coefficient associated with the blade is much smaller. Indeed, this is so because, in order to keep the overall span of the turbine (b) constant, the effective blade span has to be smaller than for the configurations with $\phi \leq 90°$. Thus, the blade extracts significantly less energy from the flow and the turbine efficiency is smaller.

If rounded blade-strut junctions are considered on turbines with a blade-strut angle of $\phi = 135°$, the turbine geometry tends toward that of the classical Darrieus turbine shape. For comparison purposes, the single-blade Darrieus turbine illustrated in Figure 21, having the same values of c, b and D as the other turbines in Section 3, has been simulated at a tip speed ratio of $\lambda = 3.25$. Note that the geometry of the blade is an approximation of a troposkien shape, similar to the shape used at Sandia National Laboratories [60, 61]. The efficiency value computed using Equations (2) to (4) for the Darrieus turbine in Figure 21 is $\eta = 27.9\%$, which is significantly smaller than the efficiency values reported in Section 3.3. However, the efficiency of the Darrieus turbine is larger than that of the turbine with the mid-span strut and that of the turbine with the quarter-span struts presented in Section 3.1.

In the literature, the efficiency of Darrieus turbines is often calculated by normalizing the power extracted by the turbine with the actual area swept by the blade; instead of using the overall frontal area $b \times D$ that was used throughout the present paper. The area covered by the turbine blade is illustrated in blue in the front view of Figure 21. Using this reference area to normalize the power extracted by the turbine is a little debatable when we compare the efficiency of Darrieus turbines with the turbines investigated in Section 3. Indeed, if we compare turbines that use the same global space $b \times D$, we should use the same reference area in order for the efficiency to be proportional to the actual power extracted by the turbines. Anyway, for the Darrieus turbine simulated here, if the power is normalized with the area illustrated in blue in Figure 21, the efficiency is $\eta = 42.3\%$. So, even with this normalization, the efficiency is still not better than for the turbine configurations with struts presented in Section 3.3.

An interesting aspect of the Darrieus turbine is that it does not require struts to attach the blades to the shaft. However, the results presented in Section 3.3 show that the struts can have a positive value of mean power coefficient (see Table 3) and can significantly increase the power extracted by the turbine blades. Therefore, the struts can be highly beneficial to the efficiency of vertical-axis turbines. Indeed, vertical-axis turbines with well-designed struts

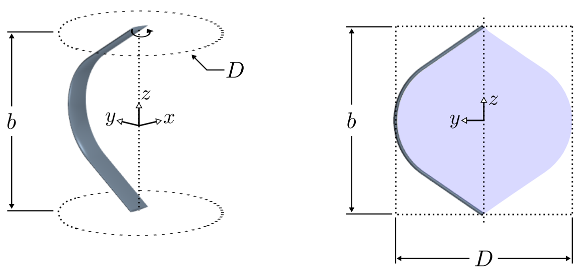

Figure 21: 3D view (left) and front view (right) of the geometry of the Darrieus turbine simulated.

could potentially outperform classical Darrieus turbines having the same overall dimensions (same values of c, b and D).

6. Conclusion

In this paper, results obtained from 25 three-dimensional URANS simulations of a single-blade vertical-axis turbine with various strut configurations are presented. The objective is to investigate the impact of the blade support structures on the performance of vertical-axis turbines.

We have shown that the turbine efficiency is highly sensitive to the position of the struts. Indeed, struts located at the blade tips are much less detrimental to the turbine efficiency than struts located at other intermediate positions along the span of the blade. Actually, the section power coefficient distribution along the blade span is significantly decreased locally around the junctions with the struts. Therefore, mid-span struts are highly detrimental to the turbine efficiency since they interfere with the blade at the spanwise position at which the blade should extract the most energy from the flow. Conversely, tip struts are more favorable since they do not ruin the mid-span region of the turbine blade.

For struts located at the blade tips, the potential of inclined struts at extracting energy from the flow has also been investigated. Typically, struts that are rotating with the turbine blades generate a drag component that results in a negative torque at the turbine shaft. Therefore, the mean power coefficient associated with the struts is negative. Interestingly, results from this paper show that for a turbine with inclined struts ($\phi = 45°$), the struts can have a positive value of mean power coefficient, thus extracting energy from the flow. However, such inclined struts interfere importantly with the turbine blade. Therefore, the efficiency value is larger for the turbine with non-inclined tip struts ($\phi = 90°$).

It is also shown that the turbine efficiency can be significantly improved if rounded junctions are used between the struts and the blade. In this paper, the turbine with non-inclined tip struts ($\phi = 90°$) having rounded blade-strut junctions at a curvature radius $R'/c = 0.5$ has an efficiency value that is more than 20% larger than the efficiency of the reference turbine without strut and 42% larger than that of the turbine with tip struts having sharp blade-strut junctions ($R'/c = 0$). This important increase in the turbine efficiency is attributed to the fact that the rounded blade-strut junctions allow to decrease significantly the kinetic energy of the vortex wake shed behind the turbine blade, and thus, allow to decrease the induced drag component. Therefore, in addition to supporting the blade structurally, the tip struts with rounded junctions also act positively on the flow, in a way somewhat similar to what winglets do for wings.

The results presented in this paper suggest that well-designed struts can be highly beneficial to the efficiency of vertical-axis turbines. However, the significant increase in mean power coefficient obtained with the rounded tip struts has here been observed on a specific single-blade turbine configuration, also operating in a uniform incoming flow. Therefore, in future works, it would be worthwhile to consider two-bladed and three-bladed turbines in order to quantify the efficiency increase when rounded tip struts are used on such turbines. It would also be interesting to further investigate the efficiency of such turbines when operating in more realistic inflow conditions (e.g., with perturbations and turbulence).

Acknowledgments

Financial support from the Natural Sciences and Engineering Research Council of Canada (NSERC Discovery Grant RGPIN-2018-04527 and CGS-D scholarship) is here gratefully acknowledged along with the important computational resources provided by Compute Canada and Calcul Québec. The authors also wish to thank Aurélien Laurencin for his help regarding the development of the meshing technique.

References

[1] M. Khan, G. Bhuyan, M. Iqbal, J. Quaicoe, Hydrokinetic energy conversion systems and assessment of horizontal and vertical axis turbines for river and tidal applications: A technology status review, Applied Energy 86 (10) (2009) 1823 – 1835.

[2] W. Tjiu, T. Marnoto, S. Mat, M. Hafidz Ruslan, K. Sopian, Darrieus vertical axis wind turbine for power generation II: Challenges in HAWT and the opportunity of multi-megawatt Darrieus VAWT development, Renewable Energy 75 (2015) 560 – 571.

[3] N. D. Laws, B. P. Epps, Hydrokinetic energy conversion: Technology, research, and outlook, Renewable and Sustainable Energy Reviews 57 (2016) 1245 – 1259.

[4] M. Islam, S. Mekhilef, R. Saidur, Progress and recent trends of wind energy technology, Renewable and Sustainable Energy Reviews 21 (2013) 456 – 468.

[5] P. J. Tavner, J. Xiang, F. Spinato, Reliability analysis for wind turbines, Wind Energy 10 (1) (2007) 1–18.
[6] H. Arabian-Hoseynabadi, H. Oraee, P. Tavner, Failure modes and effects analysis (FMEA) for wind turbines, International Journal of Electrical Power & Energy Systems 32 (7) (2010) 817 – 824.
[7] J. M. Pinar Pérez, F. P. García Márquez, A. Tobias, M. Papaelias, Wind turbine reliability analysis, Renewable and Sustainable Energy Reviews 23 (2013) 463 – 472.
[8] J. O. Dabiri, Potential order-of-magnitude enhancement of wind farm power density via counter-rotating vertical-axis wind turbine arrays, Journal of Renewable and Sustainable Energy 3 (4) (2011) 043104.
[9] M. Kinzel, Q. Mulligan, J. O. Dabiri, Energy exchange in an array of vertical-axis wind turbines, Journal of Turbulence 13 (2012) N38.
[10] M. Kinzel, D. B. Araya, J. O. Dabiri, Turbulence in vertical axis wind turbine canopies, Physics of Fluids 27 (11) (2015) 115102.
[11] I. D. Brownstein, M. Kinzel, J. O. Dabiri, Performance enhancement of downstream vertical-axis wind turbines, Journal of Renewable and Sustainable Energy 8 (5) (2016) 053306.
[12] I. D. Brownstein, N. J. Wei, J. O. Dabiri, Aerodynamically interacting vertical-axis wind turbines: Performance enhancement and three-dimensional flow, Energies 12 (14) (2019) 2724.
[13] F. Eldridge, Wind machines, MITRE energy resources and environment series, Van Nostrand Reinhold Co., 1980.
[14] R. Gosselin, G. Dumas, M. Boudreau, Parametric study of H-Darrieus vertical-axis turbines using CFD simulations, Journal of Renewable and Sustainable Energy 8 (5) (2016) 053301.
[15] A. Rezaeiha, H. Montazeri, B. Blocken, Towards optimal aerodynamic design of vertical axis wind turbines: Impact of solidity and number of blades, Energy 165 (2018) 1129 – 1148.
[16] A. Rezaeiha, H. Montazeri, B. Blocken, Characterization of aerodynamic performance of vertical axis wind turbines: Impact of operational parameters, Energy Conversion and Management 169 (2018) 45 – 77.
[17] G. Tescione, D. Ragni, C. He, C. J. Simão Ferreira, G. J. W. van Bussel, Near wake flow analysis of a vertical axis wind turbine by stereoscopic particle image velocimetry, Renewable Energy 70 (2014) 47 – 61.
[18] P. Bachant, M. Wosnik, Characterising the near-wake of a cross-flow turbine, Journal of Turbulence 16 (4) (2015) 392–410.
[19] M. Boudreau, G. Dumas, Comparison of the wake recovery of the axial-flow and cross-flow turbine concepts, Journal of Wind Engineering and Industrial Aerodynamics 165 (2017) 137 – 152.
[20] P. Chatelain, M. Duponcheel, S. Zeoli, S. Buffin, D.-G. Caprace, G. Winckelmans, L. Bricteux, Investigation of the effect of inflow turbulence on vertical axis wind turbine wakes, Journal of Physics: Conference Series 854 (1) (2017) 012011.
[21] P. Ouro, S. Runge, Q. Luo, T. Stoesser, Three-dimensionality of the wake recovery behind a vertical axis turbine, Renewable Energy 133 (2019) 1066 – 1077.
[22] V. Mendoza, P. Bachant, C. Ferreira, A. Goude, Near-wake flow simulation of a vertical axis turbine using an actuator line model, Wind Energy 22 (2) (2019) 171–188.
[23] S. Shamsoddin, F. Porté-Agel, Effect of aspect ratio on vertical-axis wind turbine wakes, Journal of Fluid Mechanics 889 (2020) R1.
[24] G. W. Rawlings, Parametric characterization of an experimental vertical axis hydro turbine, Master's thesis, The University of British Columbia (2008).
[25] B. Strom, N. Johnson, B. Polagye, Impact of blade mounting structures on cross-flow turbine performance, Journal of Renewable and Sustainable Energy 10 (3) (2018) 034504.
[26] Y. Hara, N. Horita, S. Yoshida, H. Akimoto, T. Sumi, Numerical analysis of effects of arms with different cross-sections on straight-bladed vertical axis wind turbine, Energies 12 (11) (2019) 2106.
[27] P. Bachant, M. Wosnik, B. Gunawan, V. S. Neary, Experimental study of a reference model vertical-axis cross-flow turbine, PLOS ONE 11 (9) (2016) 1–20.
[28] P. Marsh, D. Ranmuthugala, I. Penesis, G. Thomas, Three-dimensional numerical simulations of straight-bladed vertical axis tidal turbines investigating power output, torque ripple and mounting forces, Renewable Energy 83 (2015) 67 – 77.
[29] T. Villeneuve, M. Boudreau, G. Dumas, Lift enhancement and drag reduction of lifting blades through the use of end-plates and detached end-plates, Journal of Wind Engineering and Industrial Aerodynamics 184 (2019) 391 – 404.
[30] Y. Li, S. M. Calisal, Three-dimensional effects and arm effects on modeling a vertical axis tidal current turbine, Renewable Energy 35 (10) (2010) 2325 – 2334.
[31] I. Paraschivoiu, Wind Turbine Design: With Emphasis on Darrieus Concept, Polytechnic International Press, 2002.
[32] T. Villeneuve, M. Boudreau, G. Dumas, Improving the efficiency and the wake recovery rate of vertical-axis turbines using detached end-plates, Renewable Energy 150 (2020) 31 – 45.
[33] M. A. Miller, S. Duvvuri, I. Brownstein, M. Lee, J. O. Dabiri, M. Hultmark, Vertical-axis wind turbine experiments at full dynamic similarity, Journal of Fluid Mechanics 844 (2018) 707720.
[34] M. A. Miller, S. Duvvuri, W. Kelly, M. Hultmark, Rotor solidity effects on the performance of vertical-axis wind turbines at high reynolds numbers, Journal of Physics: Conference Series 1037 (2018) 052015.
[35] M. A. Miller, High Reynolds number horizontal and vertical axis wind turbine experiments, Ph.D. thesis, Princeton University (2018).
[36] P. Bachant, M. Wosnik, Effects of Reynolds number on the energy conversion and near-wake dynamics of a high solidity vertical-axis cross-flow turbine, Energies 9 (2) (2016) 73.
[37] Siemens®, Star-CCM+® V14 User's Guide, https://mdx.plm.automation.siemens.com/star-ccm-plus (2019).
[38] P. R. Spalart, S. R. Allmaras, A one-equation turbulence model for aerodynamic flows, La Recherche Aérospaciale 1 (1994) 5 – 21.
[39] P. Spalart, M. Shur, On the sensitization of turbulence models to rotation and curvature, Aerospace Science and Technology 1 (5) (1997) 297 – 302.
[40] M. Shur, M. Strelets, A. Travin, P. Spalart, Turbulence modeling in rotating and curved channels: Assessing the spalart-shur correction, AIAA Journal 38 (5) (2000) 784–792.
[41] P. R. Spalart, C. L. Rumsey, Effective inflow conditions for turbulence models in aerodynamic calculations, AIAA Journal 45 (10) (2007) 2544 – 2553.
[42] T. Kinsey, G. Dumas, Impact of channel blockage on the performance of axial and cross-flow hydrokinetic turbines, Renewable Energy 103

(2017) 239 – 254.
[43] J. S. Chow, G. G. Zilliac, P. Bradshaw, Turbulence Measurements in the Near Field of a Wingtip Vortex, Tech. Rep. NASA-TM-110418 (1997).
[44] J. S. Chow, G. G. Zilliac, P. Bradshaw, Mean and turbulence measurements in the near field of a wingtip vortex, AIAA journal 35 (10) (1997) 1561 – 1567.
[45] M. J. Churchfield, G. A. Blaisdell, A Reynolds stress relaxation turbulence model applied to a wingtip vortex flow, 49th AIAA Aerospace Sciences Meeting including the New Horizons Forum and Aerospace Exposition, Aerospace Sciences Meetings, Orlando, USA, 2011.
[46] M. J. Churchfield, G. A. Blaisdell, Reynolds stress relaxation turbulence modeling applied to a wingtip vortex flow, AIAA Journal 51 (11) (2013) 2643 – 2655.
[47] R. Gosselin, Analysis and optimization of vertical axis turbines, Ph.D. thesis, Université Laval (2015).
[48] F. Scheurich, T. M. Fletcher, R. E. Brown, Simulating the aerodynamic performance and wake dynamics of a vertical-axis wind turbine, Wind Energy 14 (2) (2011) 159–177.
[49] F. Scheurich, Modelling the aerodynamics of vertical-axis wind turbines, Ph.D. thesis, University of Glasgow (2011).
[50] A. De Marco, D. P. Coiro, D. Cucco, F. Nicolosi, A numerical study on a vertical-axis wind turbine with inclined arms, International Journal of Aerospace Engineering 2014 (2014) 1 – 14.
[51] P. G. Saffman, Vortex Dynamics, Cambridge University Press, 1993.
[52] K. Kusunose, Drag prediction based on a wake-integral method, in: 16th AIAA Applied Aerodynamics Conference, AIAA-98-2723, 1998, pp. 501 – 514.
[53] I. Kroo, Drag due to lift: Concepts for prediction and reduction, Annual Review of Fluid Mechanics 33 (1) (2001) 587–617.
[54] D. Birch, T. Lee, F. Mokhtarian, F. Kafyeke, Structure and induced drag of a tip vortex, Journal of Aircraft 41 (5) (2004) 1138–1145.
[55] D. Birch, T. Lee, Investigation of the near-field tip vortex behind an oscillating wing, Journal of Fluid Mechanics 544 (2005) 201 – 241.
[56] J. Wu, J. Hackett, D. Lilley, A generalized wake-integral approach for drag determination in three-dimensional flows, in: 17th Aerospace Sciences Meeting, AIAA 79-0279, 1979, pp. 1 – 11.
[57] G. W. Brune, P. W. Bogataj, Induced drag of a simple wing from wake measurements, in: SAE Technical Paper 901934, 1990.
[58] G. S. Winckelmans, Vortex methods, in: Encyclopedia of Computational Mechanics: Fluids, John Wiley & Sons, 2004.
[59] G. Winckelmans, R. Cocle, L. Dufresne, R. Capart, Vortex methods and their application to trailing wake vortex simulations, Comptes Rendus Physique 6 (4) (2005) 467 – 486.
[60] G. E. Reis, B. F. Blackwell, Practical approximations to a troposkien by straight-line and circular-arc segments, Tech. rep., Sandia National Laboratories, SAND74-0100, Albuquerque, NM 87115 (1975).
[61] B. F. Blackwell, R. E. Sheldahl, L. V. Feltz, Wind tunnel performance data for the Darrieus wind turbine with NACA 0012 blades, Tech. rep., Sandia National Laboratories, SAND76-0130, Albuquerque, NM 87115 (1976).